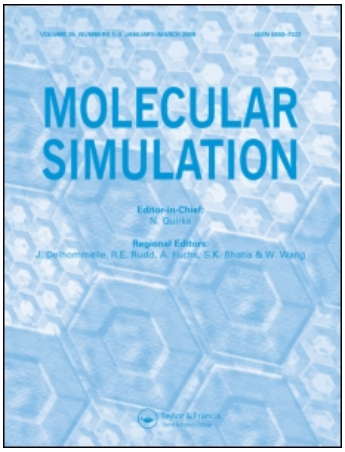

Molecular Simulation
Publication details, including instructions for authors and subscription information:
http://www.informaworld.com/smpp/title~content=t713644482

Brownian Dynamics Simulations of Electro-Rheological Fluids, II

D. M. Heyes[a]; J. R. Melrose[a]
[a] Department of Chemistry, Royal Holloway and Bedford New College, University of London, Surrey, UK

To cite this Article Heyes, D. M. and Melrose, J. R.(1990) 'Brownian Dynamics Simulations of Electro-Rheological Fluids, II', Molecular Simulation, 5: 5, 293 — 306
To link to this Article: DOI: 10.1080/08927029008022415
URL: http://dx.doi.org/10.1080/08927029008022415

Molecular Simulation, 1990, Vol. 5, pp. 293–306
Reprints available directly from the publisher
Photocopying permitted by license only

BROWNIAN DYNAMICS SIMULATIONS OF ELECTRO-RHEOLOGICAL FLUIDS, II: SCALING LAWS

D.M. HEYES and J.R. MELROSE

Department of Chemistry, Royal Holloway and Bedford New College, University of London, Egham, Surrey TW20 0EX, UK

(*Received March 1990, accepted March 1990*)

Electro-rheological fluids are technologically relevant colloidal dispersions that on application of an applied electric field manifest a yield stress and dramatic increase in viscosity. To assist optimisation of these fluids we have performed molecular simulations to understand the basic mechanisms operating in these fluids.

In this work a dispersion of field-aligned dipoles is simulated in shear flow by non-equilibrium Brownian dynamics. In agreement with experiment, a plot of the simultated relative, η_r, against a dimensionless characteristic *ER* parameter, the Mason Number, *Mn*, exhibits a plateau region (at low electric fields and/or high shear rates) prior to a steep increase in viscoisty for *Mn* smaller. Although, the simulations exhibit only an approximate data collapse according to the *Mn*. Following on from the first paper in this series we relate the origins of the *ER* effect in more detail to the temporal structural changes that take place in the fluid. We find for example, that the fluids reorganise microscopically into layers of strings of particles in the shearing plane at low *Mn*, a structure which is destroyed on entry onto the plateau in η_r at higher *Mn*. We suggest how the model could be made more realistic in future studies.

KEY WORDS: Brownian dynamics, rheology, electro-rheology.

1. INTRODUCTION

Electro-rheological, *ER*, fluids have been known and considered to be of technological importance for some time [1]. A recent review of these fluids is given by Block and Kelly [2]. A generic *ER* fluid consists of 20–40% volume fraction of solid particles of diameter (0.1–100 μm) in an insulating oil suspending medium, typically a silicone oil. Much of the discussion about the microscopic origins of the *ER* effect is largely speculation at present because the fluids are difficult to study *in situ* during typical operating conditions. The free mobility of charge within the particle measured by its polarisability, for example, seems to be crucial to the effect. The particles often, but not necessarily [2], contain a critically important percentage of included water. The particles rearrange under the influence of the electric field to form ion-conducting paths across the sample. The fluids exhibit a (largely) reversible transition from fluid to weak solid rheology on application of the electric field ($\sim MV\text{m}^{-1}$), which exhibits Bingham plastic behaviour, with yield streses up to 10 kPa. With increasing shear rate, the gel-like structure breaks down and it flows, albeit with a considerably enhanced viscosity above that of the original fluid in the absence of the field. Shear thinning of

η, and hysteresis is manifest in the stress on increasing and decreasing the strain rate, $\dot{\gamma}$.

Technological applications of these fluids included engine mounts, small clutches, ink jets and controlled tension devices - some of which are already in the market place. For practical applications it is necessary to make fluids with a low current and low variation in current with field (to limit power requirements), a low temperature variation (to give external condition stability and a small sensitivity to device warming under opeation). In addition, we require a low 'volume factor', the ratio of viscosity to the square of the yield stress, which gives the volume of fluid required to achieve a given level of mechanical control. Most fluids being studied exhibit a maximum of the *ER* effect with temperature. They also have a high power law dependence of the measured current density, J on the applied field, E, i.e., $J \propto E^k$, where $k = 2 - 5$. A further requirement is the need to stabilise the dispersions against aggregation, for a long 'shelf-life'.

The different theories of the *ER* mechanism are reviewed by Block and Kelly [2]. Prehaps the most favoured view is that the field induces dipoles on the particles. It is the dipolar interactions between the particles which then dominates the *ER* effect. The polarisation of the particles is believed to originate in the movement and redistribution of ionic charges within the particle. It is not clear whether this is a surface or bulk phenomenon, and the role of water (when present) is unclear. A competing model assigns the yield stress to the potential drop across water-conducting bridges between the particles. (A random assembly of *ER* suspended particles can be viewed as a network of coupled resistors. When a current flows through the 'network', the potential drops between the particles causes an effective attraction between them, inducing aggregation along the field lines). The electric field could cause the particles to dispel water from the bulk onto their surfaces. This could then be used to form water bridges between the particles. The surface tension of the water bridges could also play a role in the *ER* effect. The recent observation of anhydrous *ER* fluids suggests that there are, however, in all probability a number of possible mechanisms for the *ER* effect which depend on the material used. This clearly poses a problem for any simulation study that attempts to elucidate the underlying mechanism of the *ER* effect. That is, when the mechanism by which the field couples to the particles and their subsequent ('many-body') interaction, is largely a matter of guesswork at present and probably varies from material to material. At this, truly microscopic, level we cannot say very much at present. The simulation technique we use is Brownian Dynamics, *BD*. It is too 'course-grained' in both time and on distance scale to contribute on this aspect of the problem. We nevertheless believe that progress can be made using molecular simulation on this, more global, level. (We must use *BD* in order to probe the rheology [3] because it is governed by the slowest dyanmical processes in the fluid, which are the cooperative slow motions of the suspended particles). The applied field will induce an effective potential between the particles which is anisotrpic and highly attractive along the field direction. Although the precise details of this force are still largely unknown, these generic features are present in a point dipole model, in which the field induces a point dipole on each suspended particle. Coincidentally, it is also the starting point for a number of theories of the *ER* Brownian Dynamics computer simulation solves the many-body aspects of the physical system, within the constraints of the assumed force laws between the particles. We show that certain of (in fact, the major) rheological features of *ER* fluids can be reproduced by the model because certain characteristics of the force law 'scale-out' of

the determining parameters (e.g., as is measured by the Mason number [5]. The particle diameter and the nature of the repulsive interaction between the particles are not there in the Mason Number). Therefore, the simulations can still serve as a test-bed for models of the underlying mechanisms, allowing optimisation of the material parameters even through the fine details of the intermolecular forces between the suspended particles are unspecified in the simulation and are, in fact, unknown for these experimental systems.

2. SIMULATION DETAILS

Other simulations of the *ER* effect have been recently reported, mainly for small *2D* systems [6–9]. Whittle [6] made a detailed assessment of the dielectric aspects of the *ER* fluids. He used non-equilibrium brownian dynamics to evaluate the viscosity, yield stress and shear modulus as a function of field strength. The effect of the *E* field in forming fibrillated networks is now well-established by simulation in these studies. We concentrate here on the scaling properties of these fluids and also on a detailed description of the fibrille motion.

The *ER* fluid we have modelled specifically is one known to have a strong response to the *E* field. It consists of lithium polymethacrylate suspended in a silicone oil [6]. The particles are milled to diameters of $\sim 75\,\mu$m. The volume fraction of solids is 25%. The $E = 0$ ('field-free') relative viscosity of the dispersion in 5–10. The pure oil has a viscosity of 0.02 Pas at 298 K. The density of the solvent and particles was 960 kg m^{-3}.

In these simulations we generate the positions of model colloidal particles subject to an electric filed, E, in the y direction and to laminar shear flow, dv_x/dy. The molecular configurations are generated at fixed time intervals, h, using the Brownian Dynamics, *BD*, technique [10]. First we will describe the basics of *BD* and then the method of including the electric field and shear.

The Strict Langevin *BD* method employed treats the suspending medium on two independent levels. The background fluid acts to dampen out the velocities of the colloidal particles. The force on the particles by the solvent opposes the velocity through a friction coefficient, Γ. The discrete nature of the solvent is taken into account by a random force **R** acting upon the colloidal particles. The value of the random force on each particle changes with time in order to represent the net effect of the collisions of the solvent molecules on the colloidal particle. In each time interval there is an imbalance on either side of the colloidal particle, leading to the net force, **R**. This represents the net effect of the suspending medium over a fixed time interval (i.e., h).

$$\ddot{r} = F/m + R/m - \Gamma\dot{r}\,, \tag{1}$$

where r is the position of an arbitrary macromolecule, F is the systematic component of the force derived from the pair interactions betwen the colloidal particles and m is the mass of the colloidal particle (assumed all the same here). The algorithm for updating the particle positions is,

$$r_x(t + h) = r_x(t) + (F_x(t) + R_x(t, h))\, h/m\Gamma + \dot{\gamma} r_y(t) \tag{2}$$

$$r_y(t + h) = r_y(t) + (F_y(t) + R_y(t, h))\, h/m\Gamma, \tag{3}$$

$$r_z(t + h) = r_z(t) + (F_z(t) + R_z(t, h))\, h/m\Gamma, \tag{4}$$

where $\dot{\gamma}$ is the applied shear rate. Sliding (Lees-Edwards) boundary conditions are employed at the *BD* cell boundaries to maintain continuity of shear velocity profile across all space [3]. For the particle diameters considered the simulation box is a length-scale $\sim$ mm, which is typical of the gap employed in experimental electroviscometers. Therefore even through the *BD* cell is a periodic in the y-direction, a single cell has about the correct dimensions to model the number of suspended particles found between the gap between the plates typical of an experimental electroviscometer. The random force is taken from a normal distribution with standard deviation, $\langle R_\alpha^2(t, h)\rangle$, where,

$$\langle R_\alpha^2(t, h)\rangle = 2mk_B T\Gamma/h, \tag{5}$$

where $\alpha = x, y$ or z. The colloid-colloid particle potential, $\phi(r)$, has the form,

$$\phi(r_{ij}) = \epsilon(\sigma/r_{ij})^{12} + (\mu_y^2/r_{ij}^3\, 4\pi\, \epsilon_0\, \epsilon_r)\,(1 - 3r_{yij}^2/r_{ij}^2), \tag{6}$$

where the first term represents the core-core repulsion and is called the soft-sphere potential. The y component of the separation between particles i and j, r_{ij}, is r_{yij}. The magnitude and direction of each dipole is constrained to be time independent. The geometry of this flow is portrayed in Figure 1. The second term is, to first order, the intermolecular interaction due to the external field induced dipoles, μ_y. Therefore,

$$F_x = 12(r_{xij}/r_{ij})\,\epsilon\sigma^{12}/r_{ij}^{13} + 3\mu_y^2\,(r_{xij}\,4\pi\epsilon_0\,\epsilon_r)\,(1 - 3r_{jij}^2/r_{ij}^2) - 6(\mu_y^2/r_{ij}^3\,4\pi\,\eta_0\,\epsilon_r)\,(r_{xij}\,r_{yij}^2/r_{ij}^4), \tag{7}$$

$$F_y = 12(r_{yij}/r_{ij})\,\epsilon\sigma^{12}/r_{ij}^{13} + 3\mu_y^2(r_{yij}/r_{ij}^5\,4\pi\epsilon_0\,\pi_r)\,(1 - 3r_{yij}^2/r_{ij}^2) + 6\,(\mu_y^2/r_{ij}^3\,4\pi\epsilon_0\,\epsilon_r)\,(r_{yij}/r_{ij}^2 - r_{yij}^3/r_{ij}^4), \tag{8}$$

$$F_z = 12\,(r_{zij}/r_{ij})\,\epsilon\sigma^{12}/r_{ij}^{13} + 3\mu_y^2\,(r_{zij}/r_{ij}^5\,4\pi\epsilon_0\,\epsilon_r)\,(1 - 3r_{yij}^2/r_{ij}^2) - 6\,(\mu_y^2/r_{ij}^3\,4\mu\epsilon_0\,\epsilon_r)\,(r_{zij}\,r_{yij}^2/r_{ij}^4), \tag{9}$$

The *BD* simulations were performed on a cubic unit cell of volume V containing $N = 108$ model *ER* particles. To help establish scaling relationships, the calculations were performed in reduced units, i.e., $k_B T/\epsilon \to T$, and number density, $\rho = N\sigma^3/V$. Time is in $\sigma\,(m/\epsilon)^{1/2}$, shear rate is in $(\epsilon/m)^{1/2}/\sigma$, viscosity is in $(m\epsilon)^{1/2}/\sigma^2$ and stress is

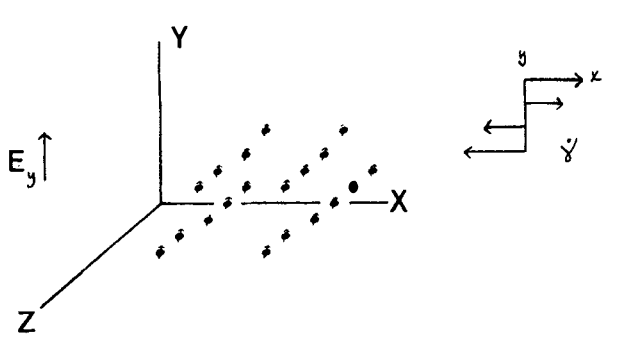

Figure 1 Sketch of the simulation geometry. The particles are shown aligned in strings at an angle to the field E direction (y), in configuration typical of the enhanced viscosity regime. The shear flow is $\dot{\gamma} = dv_x/dy$.

in $\epsilon\sigma^{-3}$. Calculated quantities are mostly given in terms of these units. The effective hard-sphere diameter, σ_{HS}/σ, of the soft-sphere potential ($\sim r^{-12}$) is [9].

$$\sigma_{HS}/\sigma = 0.9359/T^{1/2}, \tag{10}$$

The fluid density of the hard-sphere fluid at fluid-solid coexistence is, $\rho_{Hs} = 0.9428N\sigma_{HS}^3/V$. The simulations reported here were conducted at a variety of particle number densities, ρ, $\epsilon = 298k_B$ and $T = 1.0$. The solids volume fraction is $\phi = (\pi/6)\rho_{HS}$, where $\rho_{HS} = (0.9359)^3\,\rho = 0.492$, hence $\phi = 0.26$, which is close to the experimental value.

We can define a number of useful timescales. The macroparticles themselves have an 'inherent' time-scale for structural relaxation, τ_k, in the absence of the solvent which would be important if the particles were to move in a vacuum,

$$\tau_k = \sigma(m/\epsilon)^{1/2}, \tag{11}$$

where ϵ is a characteristic energy of interaction such as pair potential welldepth. There is the time-scale for velocity fluctuations of the macromolecule to decay, $\tau_p = \Gamma^{-1}$,

$$\tau_p = m/3\pi\sigma\eta_s, \tag{12}$$

where η_s is the viscosity of the pure suspending medium. There is also the timescale for local structural organisation, τ_r, the time it takes a molecule to diffuse $\sigma/2$ at extreme dilution.

$$\tau_r = 3\pi\sigma^3\,\eta/4k_b\,T, \tag{13}$$

Table 1 gives some typical values for these parameters in reduced and real units. In keeping with past work, we consider shear rates in terms of the Peclet number,

Table 1 Some typrical values of the ER system parameters. Volume fraction, $\phi = 0.26$, $\epsilon_r = 3$, $\epsilon_p = 30$, $\beta = 0.75$, $\epsilon/k_B\,T = 1$ and $T = 398$ K. We adopt the notation that xEy denotes, $x \times 10^y$. Density of solvent and particle, $= 960\,\mathrm{kgm}^{-3}$ and $\eta_s = 0.02\,Pas$. Maximum displacement per particle by the brownian term, $dr_{max}/\sigma = 0.005$, and $\epsilon/J = 0.41\ E$ - 20.

Quantity	*1*	*2*	*3*
σ/μm	0.1	1.0	75.0
m/kg	0.5E-18	0.5E-15	0.2E-9
P/Pa	4.1	0.41E-2	1.0E-8
$D_0/\mathrm{m}^2\,\mathrm{s}^{-1}$	0.22E-12	0.22E-13	0.3E-15
D_0^*	0.24E-4	0.76E-5	0.9E-6
τ_k/s	0.11E-5	0.35E-3	17
τ_p/s	0.27E-10	0.27E-8	0.9E-6
τ_B/s	0.11E-1	11	0.5E7
τ_B^*	0.24E-4	0.76E-5	0.9E-6
τ_r^*	1.0E4	3.3E4	0.3E6
η_0^*	4.4E3	1.4E4	0.12E6
h^*	0.52	1.6	14
h/s	0.57E-6	0.57E-3	242
μ^*	1.0	1.0	1.0
μ/D	1.1E4	3.5E5	2.3E8
$E/V\,\mathrm{m}^{-1}$	0.12E7	3.7E4	57.7
P_e	0.2	0.2	0.2
Mn	0.017	0.017	0.017
$\dot{\gamma}/s$	35	0.035	0.8E-7
$\dot{\gamma}^*$	0.4E-4	0.12E-4	0.-4E-5
$\dot{\gamma} \times h$	129	410	3547

$$P_e = \tau_r \dot{\gamma}/2 = 3\pi\eta_s\sigma^3 \dot{\gamma}/8k_B T, \tag{14}$$

Although, we point out that there is no universally accepted expression for P_e (it is not a universal constant). For example we find that, alternatively, $P_e = 3\pi\eta_s \sigma^3 \dot{\gamma}/4k_B T$ [11] or $P_e = \pi\eta_s\sigma^3\dot{\gamma}/8k_B T$ [12]. All we can say is that $P_e = b\pi\eta_s\sigma^3\dot{\gamma}/k_B T$, where in the various definitions, $b \sim 1$.

3. MASON NUMBER AND SCALING

In the simulation the applied field, E, influences the dynamics through a reduced dipole moment, $\mu^* \equiv \mu_v^*$. Comparing real and simulation ('reduced') units we have,

$$\phi_\mu(r) = \mu_v^2/4\pi\epsilon_0\epsilon_r r^3 \equiv \epsilon \mu^{*2} \sigma^3/r^3 \tag{15}$$

In the last term we use the reduced units of the program. Hence,

$$\mu = (4\pi\epsilon_0 \epsilon_r \epsilon\sigma^3)^{1/2} \mu^*. \tag{16}$$

Now, $\mu = E\alpha = E\alpha' 4\pi P H_0 \epsilon_r \beta$, where α is the polarisability of the particle and $\alpha' \sim (\sigma/2)^3$ is the polarisability volume. Also, $\beta = (\epsilon_p - \epsilon_r)/(\epsilon_p + 2\epsilon_r)$, where the relative dielectric constant of the particle is, ϵ_p. Hence,

$$E = 2\mu/\sigma^3 \pi\epsilon_0 \epsilon_r \beta, \tag{17}$$

Note that we use $\epsilon/k_B T = 1$ in our simulations. Through Equations (13–17) we can link the simulation parameter, μ^*, to any experimental system provided we make these assumptions.

Now we consider the dielectric and viscous properties of the experimental fluid. Recently, Marshall *et al.* [5] reported a scaling data collapse of experimental data onto plots of relative viscosity against a dimensionless parameter, the Mason Number, *Mn*. The Mason Number is defined as the ratio of the magnitudes of the viscous to the polarisation forces. The dimensionless characteristic viscous force goes as $\sim P_e$. (For particles of diameter, $\sigma > 1\,\mu$m, we can neglect the Brownian forces and assume we are in the stokesian limit). From Equation (15) we estimate the dimensionless polarisation 'force' to be,

$$W = \mu^2/(4\pi\varepsilon_0\varepsilon_r\sigma^3 k_B T), \tag{18}$$

We therefore have for $Mn = P_e/W$,

$$Mn = 4b\pi^2 \eta_s \varepsilon_0 \varepsilon_r \sigma^6 \dot{\gamma}/\mu^2, \tag{19}$$

But, as $\mu = (\pi\varepsilon_0 \varepsilon_r \beta \sigma^3)E/2$, we have,

$$Mn = (16b\eta_s/\varepsilon_0 \varepsilon_r \beta^2) \frac{\dot{\gamma}}{E^2}, \tag{20}$$

According to [5], $Mn = (\eta_s/2\varepsilon_0 \varepsilon_r \beta^2)(\dot{\gamma}/E^2)$, hence $b = 1/8$ in their definition of P_e. Therefore, from our simulations, $Mn = P_e/12\mu^{*2}$, employing our definition of P_e [3], stated in Equation (14).

A few general comments on *Mn* are appropriate here. In order to make a connection between the experimental and simulation Mason Numbers, we must specify the model of polarisation. Here we have assumed that it is in the form of a point dipole,

μ, at the centre of each particle. It is bulk polarisation (i.e., $\mu \sim \sigma^3$) rather than interfacial, which would go as $\mu \sim \sigma^2$. With this polarisation model, the particle diameter, σ, drops out of the definition of Mn. Even assuming this model, we do not know the magnitude of the dipole moment in the experimental system. This makes a quantitative comparison between experiment and simulation not possible at present.

The data of Marshall *et al.* is for a single sample subjected to varying $\dot{\gamma}$ and E. The data collapsed onto a form, $\eta_r = f(Mn)$, such that $f(Mn) \cong$ constant if $Mn > Mn_c$, a 'critical' Mason Number, Mn_c. This is where the viscous forces dominate. Also, $f(Mn) \propto Mn^{-1}$ if $Mn < Mn_c$, when the polarisation forces dominate. Experimental values for the critical Mason number, Mn_c are $\sim 10^{-1} - 1$. As the experiment only considered asingle system (e.g., the σ dependence was not explored) they only justified, $\eta_r = f(\dot{\gamma}/E^2)$. It did not test the details of the polarisation model adoped - in particular, Equation (18), which leads to a σ independent Mn, i.e., that there is no dependence on the scaling with particle size. A range of σ should be tried in future studies to establish whether this is valid. Some doubt must be cast on this simple polarisation mechanism, as it predicts a Bingham plastic flow yield stress $\tau_c \propto E^2$ [5]. In fact, at higher E fields than those studied in [5], it is often reported that τ_c crosses over from an E^2 to E dependence. So some deviation from 'bulk' polarisation seems very likely, at least at high electric field, if not below.

4. RESULTS AND DISCUSSION

The system parameters are given in section 2. They were essentially the same as those used in paper I of this series [3]. Although, as we are mainly interested here in exploring the scaling properties of these model *ER* fluids, the precise values of the system parameters are of little importance. For a given P_e, the variation of η_r with Mn was monitored. For each ρ, $\dot{\gamma}$, μ^* state point, the values quoted are averages over 10^5 time steps, with statistics assessed over 2×10^3 time step subaverages. Figures 2 and 3 portray the dependence of η_r on Mn for two different values of P_e. In Figure 2, we have $P_e = 0.2$ and Figure 3 we use $P_e = 0.05$. (Consulting Table 1, we note that the equivalent 'real' shear rates are many orders of magnitude smaller than the experimental values, $\dot{\gamma} > 1s^{-1}$). Following [5] we approximate the η_r (Mn) as two intersecting straight lines in order to determine Mn_c. A few representative error bars are presented on Figure 2. The fluctuations in η_r are particularly large in the vicinity of Mn_c, which is typical of 'critical' points in general. A comparison between Figures 2 and 3, reveals that there is a reasonable collapse of the data according to Mn for different P_e, bearing in mind the finite periodic nature of the system and that long range ordering (which is likely to be markedly N - dependent) is dominant in the *ER* effect [3,9].

The present data was further analysed into the two straight line regimes intersecting at the critical Mason Number $Mn_c \sim 0.2$ using a logarithmic scale. The latter nearly horizontal line is associated with $\eta_r = \eta_\infty$, the high shear rate limiting viscosity, which is E-independent. For $P_e = 0.2$, we find $\eta_\infty = 1.4$, $Mn_c = 2.6 \times 10^{-3}$ and a slope of the rising regime of -1.62 ± 0.21. For $P_e = 0.05$, we find $\eta_\infty = 1.4$, $Mn_c = 1.5 \times 10^{-3}$ and a slope of the rising regime of -1.41 ± 0.17. Therefore, at least on varying P_e, there is an approximate collapse of the data on the same curve. The result of Marshall *et al.* [5] give $Mn_c \sim 0.1$. Their slopes for $Mn < Mn_c$ are ~ -1, somewhat

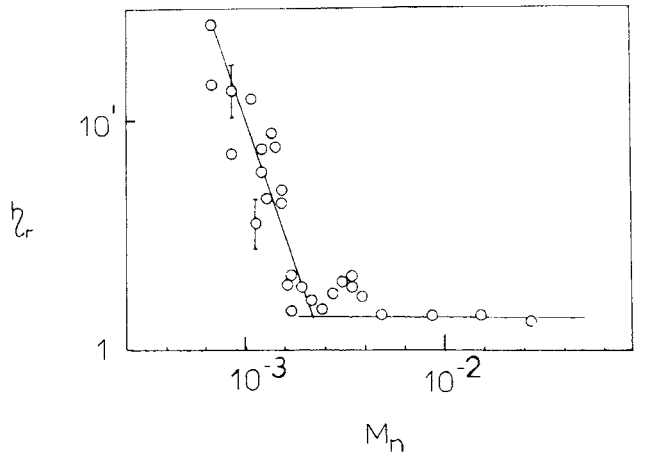

Figure 2 The relative viscosity, η_r, as a function of the Mason Number, Mn, for $P_c = 0.2$, ○ and varying the field, E.

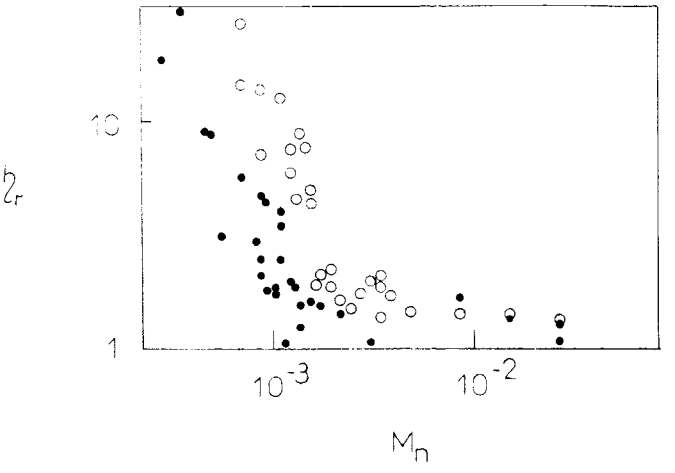

Figure 3 The relative viscosity, η_r, as a function of the Mason Number, Mn, for $P_c = 0.05$, ● and $P_c = 0.2$, ○.

lower than the simulation values. Therefore, the slopes of the simulation data indicate a faster increase than the $\eta_r \sim Mn^{-1}$ observed in experiment.

The dipole moments used in the simulations can be converted into an equivalent applied field using Equations (16) and (17). Typical values are given in Table 1. They are many orders of magnitude smaller than the experimental values. As noted above, the simulation shear rates are similarly small compared with experiment. As the Mason Number is $\propto P_v/E^2$, the simulated and experimental Mn, in fact, cover the same range. the structural states modelled will therefore be very similar because they result from the competition and balance between the shear and electric forces. The experimental fields and shear rates are too large to be simulated using the present

computational algorithms. the algorithm becomes unstable under more severe conditions (unless an impracticably small timestep is chosen). This is the same reason why dilatency ('shear thickening') has not been successfully modelled using the same method. The Brownian dynamics algorithm employed does not remain stable when the systematic interparticle forces become larger [13], as will follow higher P_e and μ^*.

We now consider the microscopic, rather than macroscopic, response to P_e and E. Shear flow can order colloidal suspensions into quasi-crystalline phases [14]. This has also been observed from *NEBD* simulation [15,16]. An electric field has a similar effect. Winslow was the first to note that the particles migrate to form chains along the field lines between the plates in *ER* fluids [1]. This ordering has also been observed in a number of recent simulations of the *ER* effect [3,10]. In the *ER* situation the ordering is more complicated because there are two perturbing 'fields' acting on the fluid simultaneously, which to a certain extent are mutually destructive of the ordered phases caused by each individually. The *ER* strings initially pointing along the y direction, resist shear flow, as the shear flow tilts them. In fact in the high Mason Number limit (i.e., low field, high shear rate) we observe strings lying parallel to the

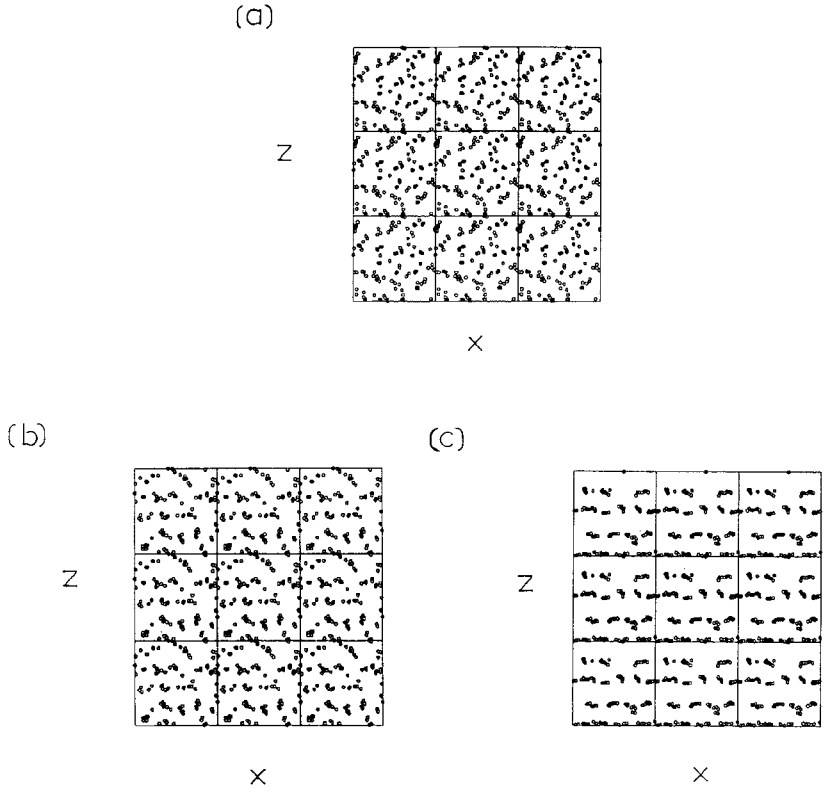

Figure 4 Three end-point configurations projected onto the xz plane, for simulations at $P_e = 0.2$, varying E. We show the *BD* cell (central square) and its 8 nearest images in the xz plane. Key: (a) $Mn = 4.6 \times 10^{-3}$, (b) $Mn = 3.3 \times 10^{-3}$ and (c) $Mn = 2.6 \times 10^{-3}$.

x-direction [15]. As the suspended particles are the stress carrying components of the suspension, these 'strings' will enhance the viscosity.

Experimentally, the *ER* effect is observed to take place on the *ms* timescale, whilst this string formation in these simulations requires many seconds (Table 1). We are not certain of the reason for this, but it could be associated with the low P_e and E employed in the simulations. This hypothesis is supported by Whittle [6], who showed using elementary hydrodynamics that, at the experimental fields employed, significant local rearrangment (particles moving $\sim \sigma$ by the electric field) can occur within a μs timescale. This is most influential in governing yield stress. A slower relaxation ($> 5\,\mu$s) is needed for a long-range fibrillation to become apparent.

Is the string formation an order parameter signalling the 'phase transition', manifest in η_r, at Mn_c? This we investigate in Figure 4 and following figures. In the enhanced viscosity regime, configurations of model suspension particles adopt a simple arrangement, which is illustrated in Figure 1. The particles form into strings in the y direction, which are collected into xy-plane layers along the the z direction. The strings are tilted by the shear flow. We did not observe this long range order in the high Mn plateau region, only for $Mn < Mn_c$ do we observe strings. Figure 4 shows three projections of this structure onto the xz plane, plotted from instantaneous configurations at the end of subaverages at $P_e = 0.2$. Figure 5 presents the corres-

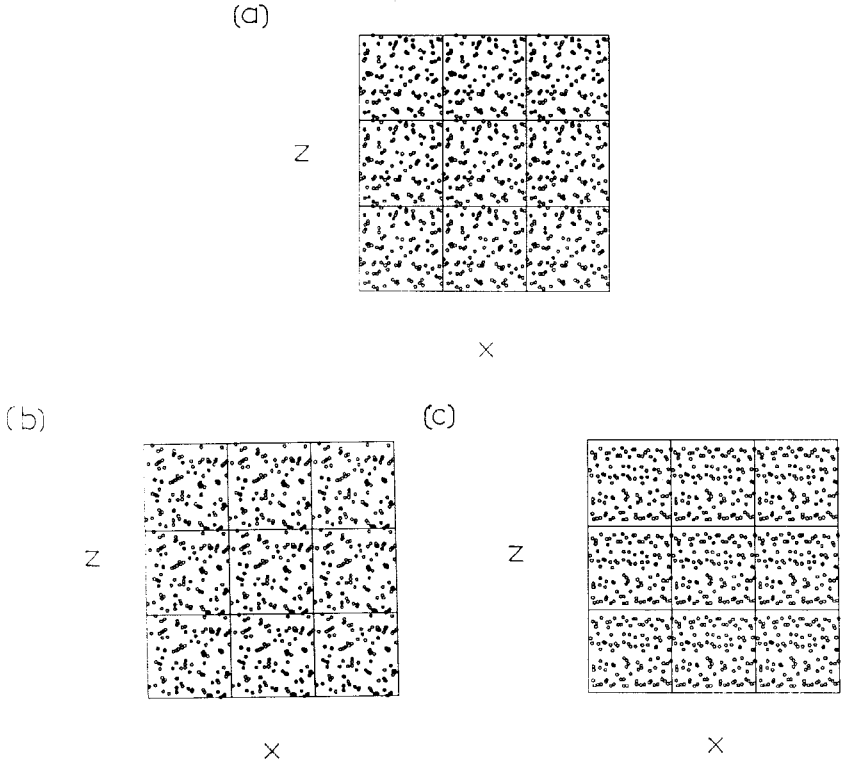

Figure 5 As for Figure 5 except $P_e = 0.05$. (a) $Mn = 2.0 \times 10^{-3}$, (b) $MN = 1.4 \times 10^{-3}$ and (c) $Mn = 7.8 \times 10^{-4}$.

ponding projections for $P_e = 0.05$. The long-range order in the liquid is obviously increasing as the Mason Number decreases.

A finer resolution of these structures is presented in Figure 6, which shows just one of these layers projected onto the xy plane. It shows two structures produced during the time evolution of this layer. Figure 6(a) captures the strings in a highly aligned and parallel arrangement. In contrast, Figure 6(b) shows the layer with the strings breaking up after reaching maximum tilt and cross-interaction betwen the strings. This is an inevitable process, which is hastened by the present point-dipole model. This is because the dipoles are constrained to point in the y direction at all times. Therefore the maximum attraction between neigbouring particles in a string occurs when the string is aligned in the y direction. As the string tilts towards the x-axis then this attraction diminishes so that the repulsive part of the pair potential will cause the string to break-up. In fact, if the string was to lie along the x-direction we would not have attraction at all between the particles.

At both $P_e = 0.05$ and $P_e = 0.2$ values, we observe that at the lower Mason Numbers there is a decrease in the number of layers from 4 to 2 per computational box. Figure 7 shows a stage in this process as there is a transition from 4 to 3 strings at $P_e = 0.2$.

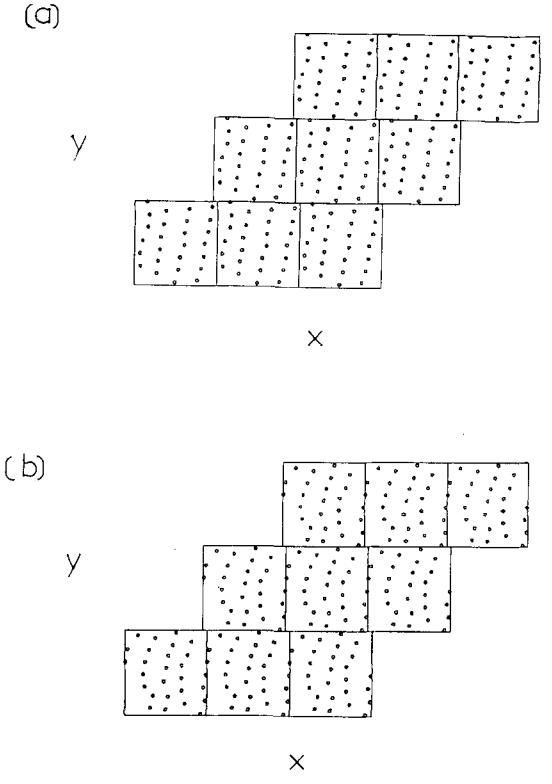

Figure 6 Two layers from the end point configuration of a $P_e = 0.2$, $Mn = 2.6 \times 10^{-3}$ simulation projected onto the xy plane. Note the distortion and break-up of the strings in (b).

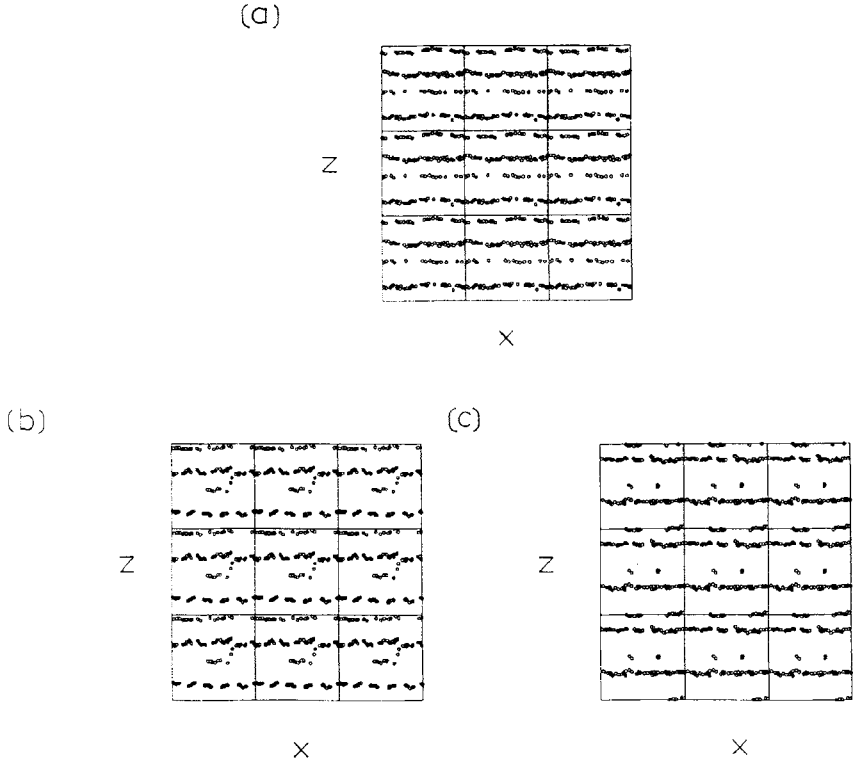

Figure 7 Three separate end-point configurations projected onto the xz plane for simulations at $P_e = 0.2$ varying the field. Key: (a) $Mn = 1.25 \times 10^{-3}$, (b) $Mn = 1.09 \times 10^{-3}$ and (c) $Mn = 9.37 \times 10^{-4}$. Note the decrease in the number of layers (4 to 3) along this sequence of MN.

5. CONCLUSIONS

We have shown that a simple point-dipole polarisation model for the suspended particles incorporated in a Brownian Dynamics simulation does reproduce the essential features of the *ER* effect. The relative viscosity exhibits shear thinning with the Mason Number as it increases from very small values to a critical Mason Number, above which the relative viscosity is essentially constant. This transition is sharper than in a recent experiment. Also, the critical Mason Number is a two orders of magnitude lower than the experimental value.

We have made a detailed analysis of the fluid configurations on either side of this boundary and show that it is accompanied by a change in long-range order. The particles reorganise from an amorphous liquid-like arrangement to the well-known fibrillated structures as the Mason Number is decreased across this critical value. Some other new features were observed on further decrease of the Mason Number, such as decrease in density of particles perpendicular to the string planes (measured in terms of the number of 'string layers').

There are other quantitaive differences between the simulations and experiment. For example, the simulated relative viscosity in the low Mason Number regime has

a higher exponent, $\sim Mn^{-1.5}$, rather than, $\sim Mn^{-1}$, which was observed in experiment. This could be a finite-size effect or a deficiency in the interaction model, an aspect currently being examined. The point dipole model employed here is obviously a considerable simplicication. Its magnitude and direction have been decoupled from the dynamics of the model *ER* fluid at each instant. This is clearly a major approximation. In addition, higher multipolar interactions are likely to become more important as the particles approach to close contact. In the present simulation model, there is no dipole induced-dipole contribution the polarisation fields. Also, the anular relaxation of the dipoles in local fields and the presence of hydrodynamic interactions have been ignored. Bonnecaze and Brady [7] have developed a far more involved model including both hydrodynamic interactions and dipole-dipole effects. As a result of the complexity of their model the computation was restricted to small N systems ($N < 50$) in two dimensions. They have sacrificed system size and 3 dimensions for a more thorough treatment of the hydrodynamics. We decided, here, to adopt a different philosophy, in employing a simple model for the interactions between the suspended particles and investigating the extent to which this will account for the experimental results. In addition, we note that there is still dispute as to what form a 'complete' treatment should be. Should this include the discreteness of the solvent? As at close contact there may only be several solvent molecules between the two particle surfaces [17]. This is not included in a full hydrodynamic treatment. We note also that whilst the layering observed here lends support to a quasi-two dimensional geometry, the destruction of these layers that we have observed on reducing the Mason Number, would obviously be unaccounted for in a $2D$ simulation and is likely to be important in determining the magnitude of the *ER* effect. Also, at present we are still uncertain of the polarisation model. It is possible that 'conducting bridges' between the suspended particles could feature in a more complete model of the *ER* effect.

Acknowledgements

D.M.H. gratefully thanks The Royal Society for the award of a Royal Society 1983 University Research Fellowship. J.R.M. thanks CASTROL Ltd. for the award of a research fellowship. Discussions with P. Bailey, D.G. Gillies, L.H. Sutcliffe and N. Webb are gratefully acknowledged.

References

[1] W.M. Winslow, "Induced fibration of suspensions", *J. Appl. Phys.*, **20**, 1137 (1949).
[2] H. Block and J.P. Kelly, "Electro-rheology", *J. Phys. D: Appl. Phys.*, **21**, 1661 (1988).
[3] P. Bailey, D.G. Gillies, D.M. Heyes and L.H. Sutcliffe, "Experimental and simulation studies of electro-rheology", *Mol. Sim.*, **4**, 137 (1989).
[4] P.M. Adriani and A.P. Gast, "A microscopic model of electrorheology", *Phys. Fluids*, **31**, 2757 (1988).
[5] L. Marshall, C.F. Zukowski IV and J.W. Goodwin, "Effects of electric fields on the rheology of non-aqueous concentrated suspensions", *J. Chem. Soc. Faraday Trans I*, **85**, 2785 (1989).
[6] M. Whittle, "Computer simulation of an electro-rheolgical fluid", to be published.
[7] R.T. Bonnecaze and J.F. Brady, "Dynamic simulation of a suspension of dielectric particles forming an electrorheological fluid", to be published in *Proc. of the II International conference of electrorheological Fluids*. Raleigh 1989, Eds H Conrad, A.F. Sprecher and J.D. Carlson.
[8] D.J. Klingenberg and C.F. Zukoski IV, "Structure formation in electrorheological fluids", to be published in *Proc. of the II International conference on electrorheolgical Fluids*, Raleigh 1989, Eds H Conrad, A.F. Sprecher and J.D. Carlson.

[9] D.J. Klingenberg, F. van Swol and C.F. Zukowski, "Dynamic simulation of electrorheological suspensions", *J. Chem. Phys.*, **91**, 7888 (1989).
[10] D.M. Heyes. "Rheology of molecular liquids and concentrated suspensions by microscopic dynamical simulations", *J. Non-Newt. Fl. Mech.*, **27**, 47 (1988).
[11] J.C. van der Werff and C.G. de Kruiff, "Hard-sphere colloidal dispersions: the scaling of rheological properties with particle size, volume fraction, and shear rate", *J. of Rheol.*, **33**, 421 (1989).
[12] J. Mewis, W.J. Frith, T.A. Strivens and W.B. Russel, "The rheology of suspensions containing polymerically stabilized particles", in *AICHE Journal*, **35**, 415 (1989).
[13] R.W. Pastor, B.R. Brooks and A. Szabo, "A analysis of the accuracy of Langevin and molecular dynamics algorithms", *Mol. Phys.*, **65**, 1409 (1988).
[14] B.J. Ackerson and N.A. Clark, "Shear-induced partial translational ordering of a colloidal solid", *Phys. Rev. A*, **30**, 906 (1984).
[15] D.M. Heyes, "Shear thinning of dense suspensions modelled by brownian dynamics", *Phys. Lett. A*, **132**, 399 (1988).
[16] W. Xue and G.S. Grest, "Shear-Induced alignment of colloidal particles in the presence of shear flow", *Phys. Rev. Lett.*, **64**, 419 (1990).
[17] L.V. Woodcock, private communication, 1989.